


## Pseudo Dirac nodal sphere semimetal

Jianfeng Wang,<sup>1</sup> Yizhou Liu,<sup>2</sup> Kyung-Hwan Jin,<sup>3</sup> Xuelei Sui,<sup>2,1</sup> Lizhi Zhang,<sup>1</sup> Wenhui Duan,<sup>2,4</sup> Feng Liu,<sup>3,4</sup> and Bing Huang<sup>1,\*</sup><sup>1</sup>Beijing Computational Science Research Center, Beijing 100193, China<sup>2</sup>Department of Physics and State Key Laboratory of Low-Dimensional Quantum Physics, Tsinghua University, Beijing 100084, China<sup>3</sup>Department of Materials Science and Engineering, University of Utah, Salt Lake City, Utah 84112, USA<sup>4</sup>Collaborative Innovation Center of Quantum Matter, Beijing 100084, China (Received 2 April 2018; revised manuscript received 7 September 2018; published 26 November 2018)

Topological semimetals (TSMs) in which conduction and valence bands cross at zero-dimensional (0D) Dirac nodal points (DNPs) or 1D Dirac nodal lines (DNLs), in 3D momentum space, have recently drawn much attention due to their exotic electronic properties. Here, we generalize the TSM state further to a higher-dimensional Dirac nodal sphere (DNS) or pseudo DNS (PDNS) state, with the band crossings forming a 2D closed or approximate sphere at the Fermi level. This TSM state can exhibit unique electronic properties, making DNS/PDNS a type of fermion beyond the DNP/DNL paradigm. In realistic crystals, we demonstrate two possible types of PDNS states underlain by different crystalline symmetries, which are characterized with a spherical backbone consisting of multiple DNLs and approximate band degeneracy in between the DNLs. We identify all the possible band crossings with pairs of 1D irreducible representations to form the PDNS states in 32 point groups. Importantly, we discover that strained  $MH_3$  ( $M = Y, Ho, Tb, Nd$ ) and  $Si_3N_2$  are material candidates to realize these two types of PDNS states, respectively. As a high-symmetry-required state, the PDNS semimetal can be regarded as the “parent phase” for other topological gapped and gapless states.

DOI: [10.1103/PhysRevB.98.201112](https://doi.org/10.1103/PhysRevB.98.201112)

The rise of topological insulators [1,2] has brought the field of topological states to the center stage of condensed matter physics. Recent attention has been focused on topological semimetals (TSMs), which can support quasiparticles either analogous to elementary particles in high-energy physics or previously unknown [3–7]. To date, the well-known TSMs include Dirac, Weyl, and nodal-line semimetals [5–14]. The Dirac semimetals [5–7] have zero-dimensional (0D) band crossings, i.e., the Dirac nodal points (DNPs), whose Fermi surface consists of isolated points in the Brillouin zone (BZ) [upper panel, Fig. 1(a)]. The low-energy excitations (LEEs) of DNP semimetals have some unique properties such as chiral anomaly and surface states with Fermi arcs. The nodal-line semimetals [6–14] feature 1D band crossings at the Fermi surface with closed Dirac nodal lines (DNLs) in the BZ [upper panel, Fig. 1(b)]. The DNL semimetals host special drumhead surface states, which provide an important platform to realize a strong electron correlation effect. Very recently, a nodal surface has been also proposed, with the band crossing points forming a 2D plane [15,16].

Unlike DNPs and DNLs, conceptually it is also possible that the linear band crossing occurs on a 2D closed surface [17,18], forming a Dirac nodal sphere (DNS) or pseudo DNS (PDNS, an approximate DNS with the same LEE; see below for details) at the Fermi energy, as shown in the upper panel of Fig. 1(c). On a DNS/PDNS, each point is a crossing point between two bands with linear dispersion along the

surface normal direction, which can be expressed as

$$H(k') = \hbar v_F k' \sigma_z, \quad (1)$$

where  $k' = k - k_0$  is the component of the wave vector normal to the Fermi surface,  $k_0$  is the radius of DNS,  $v_F$  is the Fermi velocity, and  $\sigma_z$  is the Pauli matrix denoting the two crossing bands.

Since the LEE dimensionality of DNS is fundamentally different from that of DNP (DNL), the DNS semimetal can possess very unique electronic properties. For example, it has a significantly different density of states (DOS):  $\text{DOS} \propto (E - E_F)^2$  for a DNP [lower panel, Fig. 1(a)],  $\text{DOS} \propto |E - E_F|$  for a DNL [lower panel, Fig. 1(b)], and  $\text{DOS} \propto \text{const}$  [19] for a DNS [lower panel, Fig. 1(c)]. The constant DOS may make the DNS semimetals exhibit some unusual field responses and applications, e.g., a significantly stronger quantum oscillation and peculiar plasmon excitations. Thus, the DNS fermion can be recognized as a type of fermion beyond the DNP/DNL paradigm.

One intriguing question is how to realize this DNS state in realistic materials. Although the (Weyl) nodal sphere state has been theoretically proposed based on global symmetries [17,18], it is too difficult, if not impossible, to be realized in real crystals having discrete point group symmetries. Here, we present an effective approach to generate the PDNS state in accessible crystalline symmetries. In general, a band crossing located on high-symmetry lines/planes is stable against band repulsion only when the wave functions belong to different eigenstates of some crystalline symmetry operation. For an ideal DNS, the band degeneracy should occur at an arbitrary momentum point (say, the  $P$  point) on the sphere. But generally the coupling between two crossing bands at  $P$  cannot

\*Bing.Huang@csr.c.ac.cn

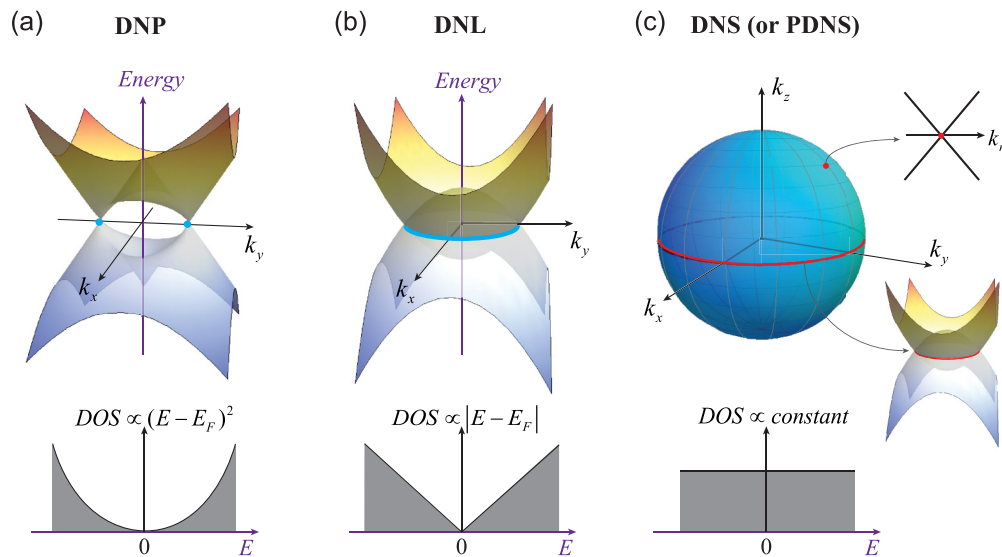


FIG. 1. Comparison between (a) Dirac nodal point (DNP), (b) Dirac nodal line (DNL), and (c) Dirac nodal sphere (DNS) or pseudo DNS (PDNS) for their distinct Fermi-surface geometries (upper panels) and density of states (lower panels) around the Fermi level. An arbitrary point (loop) on DNS can be regarded as a “constrained” DNP (DNL).

be strictly avoided. Interestingly, near some high-symmetry  $k$  points, we discover that under some appropriate conditions the special crystalline symmetries will only allow for high-order interaction terms (HITs) of  $k$  between two crossing bands, which can be sufficiently weak and hence negligible. In this case, a PDNS state forms. As illustrated in Fig. 2, the PDNS state is characterized with a spherical backbone consisting of multiple crossing DNLs while band degeneracy in between the DNLs is approximately maintained by weak interactions. It is emphasized that the LEE of a PDNS is the same as an ideal DNS, albeit only a key subset of crossing points (DNLs) formed as the spherical backbone of the PDNS is topologically protected.

We identify two sets of crystalline symmetries under time-reversal symmetry (TRS) to realize the desired PDNS states: type I for inversion plus at least two mirror ( $\hat{P} + 2\hat{M}$ ) symmetries and type II for at least three mirror ( $3\hat{M}$ ) symmetries. Importantly, we identify all the possible band crossings with

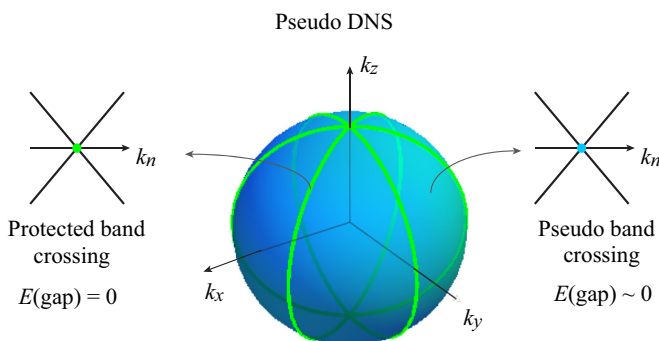


FIG. 2. Illustration of the pseudo DNS (PDNS) state. The band crossing on multiple DNLs formed as the spherical backbone of PDNS (green points) is topologically protected, while band degeneracy in between the DNLs (cyan points) is approximately maintained by weak interactions, which is called pseudo band crossing.

pairs of 1D irreducible representations (IRRs) to form these two types of PDNS states in 32 point groups. Employing first-principles calculations, we further show that  $M\text{H}_3$  ( $M = \text{Y, Ho, Tb, Nd}$ ) and  $\text{Si}_3\text{N}_2$  are type-I and type-II PDNS semimetals under certain strains, respectively. They both have drumhead surface states independent of surface orientations.

We consider a two-band model in a system with TRS and ignore the spin degree of freedom [19]. The type-I PDNS has  $\hat{P} + 2\hat{M}$  symmetries. At a high-symmetry point, e.g., the  $\Gamma$  point, if the two bands have opposite parities for  $\hat{P}$  and opposite mirror eigenvalues for two different mirror operators ( $\hat{M}_x$  and  $\hat{M}_y$ ), the Hamiltonian can be written as [19]

$$H(\mathbf{k}) = (M - Bk^2)\sigma_z + \delta k_x k_y k_z \sigma_y, \quad (2)$$

where  $k^2 = k_x^2 + k_y^2 + k_z^2$ , and  $\sigma_{y,z}$  are Pauli matrices for the two bands. Under the band inversion condition ( $MB > 0$ ),  $\hat{P} + 2\hat{M}$  will strictly create three crossing nodal lines in the  $k_{x,y,z} = 0$  planes [11, 12]. Away from the three planes, there would be a gap induced by HIT of  $g_2(\mathbf{k})$ , but it can be sufficiently tiny and negligible for small  $k$  near the high-symmetry point. Consequently, the band crossings can extend to form a PDNS. Around a crossing point, the LEE quasiparticles can be described by Eq. (1) with  $k_0 = \sqrt{M/B}$  and  $v_F = -2\sqrt{MB}$ .

The minimum symmetries required for the type-I PDNS are  $\hat{P} + 2\hat{M}$  plus TRS. Meanwhile, the two inverted bands at the high-symmetry point should belong to two different 1D IRRs, i.e.,  $R_1$  and  $R_2$ , which have opposite parities and mirror eigenvalues. It is emphasized that the required number of symmetric mirror planes for PDNS can be more than two, e.g., three, four, or even six. Applying these criteria to 32 point groups, we identify that six point groups can host type-I PDNS, and all the associated possible pairs of 1D IRRs are listed in Table I.

The type-II PDNS has  $3\hat{M}$  symmetries. One may take three mirrors as  $3\hat{\sigma}_v$  of the  $C_{3v}$  point group. If the two crossing bands have opposite eigenvalues for  $3\hat{\sigma}_v$ , the Hamiltonian can

TABLE I. Two different types of PDNS realized by different point groups with all the possible 1D IRRs, and the proposed materials (without SOC effect), where  $MH_3$  ( $M = Y, Ho, Tb, Nd$ ),  $Tl_5Se_2Br$ ,  $Tl_4PbTe_3$ ,  $Tl_4SnTe_3$ , and  $Si_3N_2$  require strains to realize PDNS states.

PDNS type	Point group	1D IRRs of two bands $\{R_1, R_2\}$	Materials
Type I	$D_{2h}$	$\{A_g, A_u\}, \{B_{ig}, B_{iu}\},$ $i = 1, 2, 3$	LaN, CaTe YH <sub>3</sub> , HoH <sub>3</sub> , TbH <sub>3</sub> , NdH <sub>3</sub>
	$D_{4h}$	$\{A_{ig}, A_{iu}\}, \{B_{ig}, B_{iu}\},$ $\{A_{ig(u)}, B_{ju(g)}\}, i, j = 1, 2$	
	$D_{3d}$	$\{A_{ig}, A_{iu}\}, i = 1, 2$	
	$D_{6h}$	$\{A_{ig}, A_{iu}\}, \{B_{ig}, B_{iu}\},$ $\{A_{ig(u)}, B_{ju(g)}\}, i, j = 1, 2$	
	$T_h$	$\{A_g, A_u\}$	
	$O_h$	$\{A_{ig}, A_{ju}\}, i, j = 1, 2$	
	Type II	$C_{4v}$	
$D_{4h}$		$\{A_{1g(u)}, A_{2g(u)}\},$ $\{B_{1g(u)}, B_{2g(u)}\}$	
$C_{3v}$		$\{A_1, A_2\}$	
$D_{3d}$		$\{A_{1g(u)}, A_{2g(u)}\}$	
$C_{6v}$		$\{A_1, A_2\}, \{B_1, B_2\},$ $\{A_i, B_j\}, i, j = 1, 2$	
$D_{3h}$		$\{A'_1, A'_2\}, \{A''_1, A''_2\},$ $\{A'_1, A''_1\}, \{A'_2, A''_2\}$	
$D_{6h}$		$\{A_{1g(u)}, A_{2g(u)}\}, \{B_{1g(u)}, B_{2g(u)}\},$ $\{A_{ig(u)}, B_{jg(u)}\}, i, j = 1, 2$	
$T_d$		$\{A_1, A_2\}$	
$O_h$		$\{A_{1g(u)}, A_{2g(u)}\}$	
			$\beta\text{-Si}_3\text{N}_2$ $\alpha\text{-Si}_3\text{N}_2$

be written as [19]

$$H(\mathbf{k}) = (M - Bk^2)\sigma_z + \delta(k_x^3 - 3k_x k_y^2)\sigma_y. \quad (3)$$

Once again, strictly speaking, it creates three crossing DNLs, which are related with each other by  $C_3$  rotational symmetry. However, away from the three planes, the small gap induced by HIT of  $g_2(\mathbf{k})$  can be neglected near the high-symmetry point. Thus, we obtain the PDNS under the type-II symmetry constraints.

The minimum symmetries required for the type-II PDNS are  $3\hat{M}$  plus TRS. At the high-symmetry point, the two inverted bands with two different 1D IRRs should have opposite mirror eigenvalues. Also, the required number of symmetric mirror planes for the type-II PDNS can be more than three, e.g., four or six. Applying this criterion to 32 point groups, we determine that nine point groups can potentially host type-II PDNS, and all the associated pairs of 1D IRRs are listed in Table I.

Next, we discuss the topological properties of PDNS. For an ideal DNS semimetal, its topological invariant can be defined on a 0D point enclosing manifold [16–18,37]. Considering two momentum points  $\mathbf{k}_{in}$  and  $\mathbf{k}_{out}$  located anywhere inside and outside the ideal DNS, its topological invariant can be defined as  $\Delta c = [c(\mathbf{k}_{in}) - c(\mathbf{k}_{out})]/2$ , where  $c(\mathbf{k}) = \sum_{n \in occ} \langle u_n(\mathbf{k}) | \hat{X} | u_n(\mathbf{k}) \rangle$  is a quantum number of symmetry operator  $\hat{X}$  for all the occupied bands. However, our PDNS

is not an ideal one so that  $c$  cannot be well defined at an arbitrary  $\mathbf{k}$  point; instead, it needs to be defined within a plane that contains the loop formed by DNLs. Since the DNLs are underlain by the crystal symmetries as we discussed above, one can selectively choose those high-symmetry  $\mathbf{k}$  points accordingly. For type-I PDNS that has inversion symmetry,  $c$  can be defined as the sum of parity for every occupied band at the time-reversal invariant point ( $\hat{X} = \hat{P}$ ); for type-II PDNS,  $c$  can be defined as the sum of mirror eigenvalues at the mirror-invariant plane ( $\hat{X} = \hat{M}$ ).

We emphasize that the nontrivial (nonzero)  $\Delta c$  defined here cannot protect the whole PDNS against being gapped under a symmetry preserving perturbation, but it can protect the existence of multiple crossing NLS (a necessary condition for achieving the PDNS state). Furthermore, if a perturbation preserves all the required symmetries and maintains a weak band inversion, the band degeneracy of the whole PDNS will be kept. In addition, the zero codimensionality of PDNS cannot, in principle, guarantee any boundary state [16]. The surface states if generated will interact with the bulk states not to be localized on the boundary. However, the drumhead surface states arising from the multiple crossing DNLs are protected on the boundary, except they may appear somewhat fuzzy due to overlapping with the bulk states.

It is noted that we did not include the spin degree of freedom in our PDNS model discussions. All the predicted materials listed in Table I are strictly crossing-nodal-line semimetals with an extremely tiny energy gap ( $< 2$  meV) at a general band crossing point  $P$  (induced by HITs of  $k$ ) [19,38]. Without the SOC effect, all the candidates listed in Table I can be treated as PDNS semimetals in terms of their LEE properties. For LaN, CaTe,  $Tl_5Se_2Br$ ,  $Tl_4PbTe_3$ ,  $Tl_4SnTe_3$  (Table I), however, the SOC effects are sufficiently strong to reduce the PDNS phase to the DNP (or topological insulator) phase [19]. Interestingly, for  $MH_3$  ( $M = Y, Ho, Tb, Nd$ ) and  $\alpha/\beta\text{-Si}_3\text{N}_2$ , their PDNS phases (under certain strains) are robust against the SOC effect [19], as demonstrated in the following discussions.

Metal hydrides have been studied extensively for superconductivity and metal-insulator transitions under pressure [39–41]. YH<sub>3</sub> adopts the HoD<sub>3</sub> structure [42] having the space group  $P\bar{3}c1$  (No. 165), as shown in Fig. 3(a). It has inversion symmetry, threefold rotation symmetry, and three glide planes related by  $C_3$  rotation. It is a normal semiconductor whose conduction band minimum (CBM) and valence band maximum (VBM) at the  $\Gamma$  point belong to the  $A_{2g}$  and  $A_{2u}$  representations of  $D_{3d}$  (without SOC effect) [19], respectively. Based on our PDNS model (Table I), it is expected to have a type-I PDNS when its  $A_{2g}$  and  $A_{2u}$  bands are weakly crossed. Indeed, we found that YH<sub>3</sub> can be transformed into a gapless PDNS semimetal when a compressive uniaxial strain ( $\varepsilon_c < -3.8\%$ ) is applied along the  $c$  axis [19], as shown in Fig. 3(b). As shown in Fig. 3(c), the gapless band crossing maintains along any arbitrary  $\mathbf{k}$  direction around  $\Gamma$ , with a negligible gap ( $< 0.5$  meV) induced by HITs. We note that the HITs between the two crossing bands are related with the band inversion strength. The condition for the HITs to be negligibly small can always be guaranteed by an appropriate  $\varepsilon_c$  [19]. Given the opposite parities of  $\hat{P}$  and  $\hat{M}$  eigenvalues of three glide planes [labeled in Fig. 3(c)], the band crossing

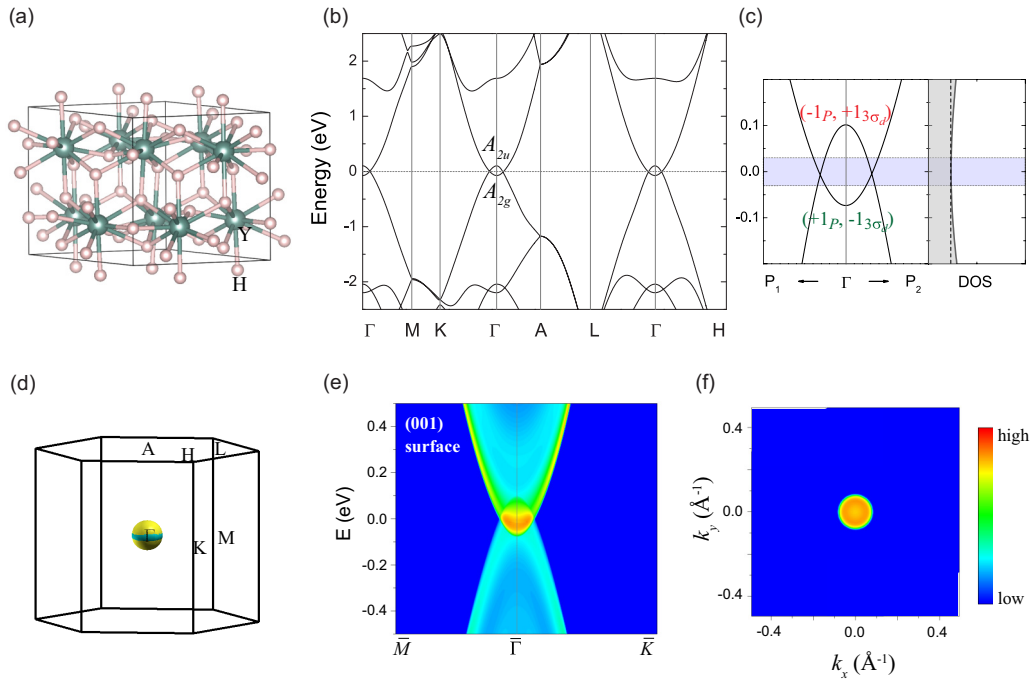


FIG. 3. (a) Crystal structure of  $\text{YH}_3$ . (b) Band structure of  $\text{YH}_3$  under  $\varepsilon_c = -6\%$  (without SOC) using Heyd-Scuseria-Ernzerhof functional (HSE06) calculations. (c) Left panel: Magnified band structure along two arbitrary directions around  $\Gamma$  ( $P_1$  and  $P_2$  are two arbitrary  $\mathbf{k}$  points in BZ), where the opposite eigenvalues of parity and glide planes for two crossing bands are labeled. Right panel: DOS, where the dashed line denotes a constant DOS. (d) The Fermi surface of  $\text{YH}_3$  in BZ. Cyan (yellow) surface denotes hole (electron) pockets at the Fermi level. (e) and (f) Surface projected bands and Fermi surfaces for (001) surface of  $\text{YH}_3$ .

for type-I PDNS is approximately protected by  $D_{3d}$  symmetry with a calculated  $\Delta c = 1$ . The calculated constant DOS in the energy range of nearly linear dispersion [Fig. 3(c)] agrees well with that in Fig. 1(c). The spherical Fermi surface of strained

$\text{YH}_3$  formed by the band crossing is shown in Fig. 3(d), and its size  $k_0$  can be tuned by  $\varepsilon_c$  [19]. Since the band crossing is not exactly located at the Fermi energy, the Fermi surface presents hole (electron) pockets near (away from) the  $\Gamma MK$

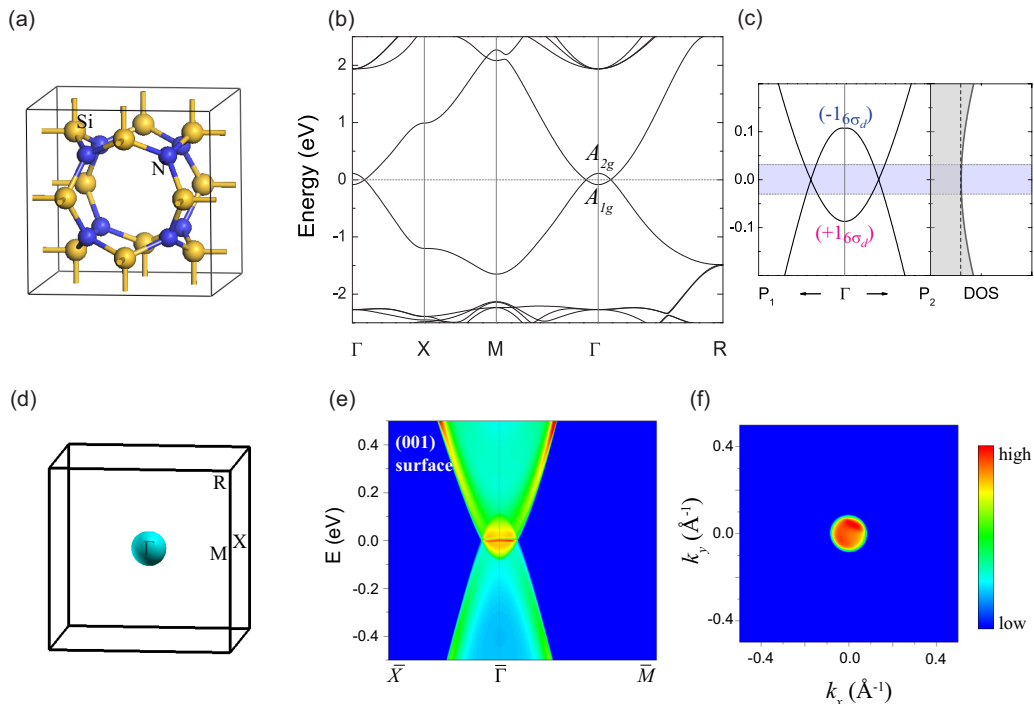


FIG. 4. (a)–(f) Same as Fig. 3 but for type-II  $\alpha\text{-Si}_3\text{N}_2$ .

plane. These results are not affected by the SOC effect [19], as reflected by a tiny SOC gap ( $<1.5$  meV).

Drumhead surface states arising from the crossing nodal lines are shown in Figs. 3(e) and 3(f). Due to the interaction with the projected bulk states, the drumhead surface states appear a little fuzzy. Different from the usual DNL semimetal, the drumhead surface states of  $\text{YH}_3$  are independent of its surface orientations, i.e., the [001]- and [010]-oriented surface states are almost the same [19], because of its near spherical band crossing.

As a candidate material for a type-II PDNS semimetal,  $\alpha\text{-Si}_3\text{N}_2$  [43] adopts the cubic structure having the space group  $Pm\bar{3}m$  (No. 221), as shown in Fig. 4(a).  $\alpha\text{-Si}_3\text{N}_2$  is a normal semiconductor [19], whose VBM and CBM belong to the  $A_{2g}$  and  $A_{1g}$  representations of the  $O_h$  point group, respectively. Based on our analysis (Table I), a type-II PDNS phase can be achieved when these two bands are crossed. We found that a sufficiently large triaxial compressive strain of  $\varepsilon < -5\%$  (corresponds to a hydrostatic pressure of  $\sim 30$  GPa) can induce this desired phase [19], as shown in Fig. 4(b). Near the Fermi level, band crossing persists along any arbitrary direction around  $\Gamma$  [Fig. 4(c)]. Importantly, although the two crossing bands have the same parities, the eigenvalues of six mirror planes for these two bands are of opposite sign [labeled in Fig. 4(c)]. Thus,  $\alpha\text{-Si}_3\text{N}_2$  is a type-II PDNS with multiple DNLs protected by the mirror symmetries (the calculated  $\Delta c = 1$ ). As expected, it has a constant DOS in the energy

range of nearly linear dispersion [Fig. 4(c)], a spherical Fermi surface [Fig. 4(d)], and surface-independent drumhead surface states [Figs. 4(e) and 4(f)]. The PDNS phase in  $\alpha\text{-Si}_3\text{N}_2$  is robust with a very small SOC gap ( $<0.1$  meV) [19].

As a high-symmetry-required state, the PDNS semimetal can be considered as the “parent phase” for other gapped and gapless topological states. For instance, certain perturbations may tune the HIT transforming a PDNS semimetal into a nodal-line semimetal [19]; a sufficiently large SOC may convert a PDNS semimetal into a DNP semimetal or a topological insulator [19]. Moreover, because of the finite DOS in the linear band crossing region [Fig. 1(c)], Coulomb repulsion might drive the PDNS phase to induce various quantum orders [44]. Especially, the existence of superconductivity in  $\text{MH}_3$  under pressure (strain) [39,40] may provide a unique platform to study the interplay between the PDNS fermions and superconductivity.

The authors thank L. Lim, S. W. Gao, and S.-H. Wei for helpful discussions. J.W. and B.H. acknowledge the support from NSFC (Grant No. 11574024) and NSAFU1530401. K.J. and F.L. acknowledge the support from U.S. DOE (Grant No. DE-FG02-04ER46148). Y.L., X.S., and W.D. acknowledge support from MOST of China (Grant No. 2016YFA0301001) and NSFC (Grants No. 11674188 and No. 11334006). Parts of the calculations were performed at Tianhe2-JK at CSRC.

- 
- [1] M. Z. Hasan and C. L. Kane, *Rev. Mod. Phys.* **82**, 3045 (2010).
- [2] X.-L. Qi and S.-C. Zhang, *Rev. Mod. Phys.* **83**, 1057 (2011).
- [3] C.-K. Chiu, J. C. Y. Teo, A. P. Schnyder, and S. Ryu, *Rev. Mod. Phys.* **88**, 035005 (2016).
- [4] A. Bansil, H. Lin, and T. Das, *Rev. Mod. Phys.* **88**, 021004 (2016).
- [5] N. P. Armitage, E. J. Mele, and A. Vishwanath, *Rev. Mod. Phys.* **90**, 015001 (2018).
- [6] A. A. Burkov, M. D. Hook, and L. Balents, *Phys. Rev. B* **84**, 235126 (2011).
- [7] H. Weng, X. Dai, and Z. Fang, *J. Phys.: Condens. Matter* **28**, 303001 (2016).
- [8] C. Fang, H. Weng, X. Dai, and Z. Fang, *Chin. Phys. B* **25**, 117106 (2016).
- [9] S.-Y. Yang, H. Yang, E. Derunova, S. S. P. Parkin, B. Yan, and M. N. Ali, *Adv. Phys. X* **3**, 1414631 (2018).
- [10] Y. Kim, B. J. Wieder, C. L. Kane, and A. M. Rappe, *Phys. Rev. Lett.* **115**, 036806 (2015).
- [11] R. Yu, H. Weng, Z. Fang, X. Dai, and X. Hu, *Phys. Rev. Lett.* **115**, 036807 (2015).
- [12] H. Weng, Y. Liang, Q. Xu, R. Yu, Z. Fang, X. Dai, and Y. Kawazoe, *Phys. Rev. B* **92**, 045108 (2015).
- [13] M. Zeng, C. Fang, G. Chang, Y.-A. Chen, T. Hsieh, A. Bansil, H. Lin, and L. Fu, [arXiv:1504.03492](https://arxiv.org/abs/1504.03492).
- [14] Y. Du, F. Tang, D. Wang, L. Sheng, E.-J. Kan, C.-G. Duan, S. Y. Savrasov, and X. Wan, *npj Quantum Mater.* **2**, 3 (2017).
- [15] Q.-F. Liang, J. Zhou, R. Yu, Z. Wang, and H. Weng, *Phys. Rev. B* **93**, 085427 (2016).
- [16] W. Wu, Y. Liu, S. Li, C. Zhong, Z.-M. Yu, X.-L. Sheng, Y. X. Zhao, and S. A. Yang, *Phys. Rev. B* **97**, 115125 (2018).
- [17] T. Bzduszek and M. Sigrist, *Phys. Rev. B* **96**, 155105 (2017).
- [18] O. Türker and S. Moroz, *Phys. Rev. B* **97**, 075120 (2018).
- [19] See Supplemental Material at <http://link.aps.org/supplemental/10.1103/PhysRevB.98.201112> for details of the derivations of DOS, two types of PDNS models, computational methods, crystal structures, band structures with and without SOC of all predicted PDNS material candidates in Table I, and strain effect on  $\text{YH}_3$  and  $\alpha\text{-Si}_3\text{N}_2$ , which also includes Refs. [20–36].
- [20] G. Kresse and J. Furthmüller, *Comput. Mater. Sci.* **6**, 15 (1996).
- [21] G. Kresse and J. Furthmüller, *Phys. Rev. B* **54**, 11169 (1996).
- [22] P. E. Blöchl, *Phys. Rev. B* **50**, 17953 (1994).
- [23] J. P. Perdew, K. Burke, and M. Ernzerhof, *Phys. Rev. Lett.* **77**, 3865 (1996).
- [24] J. Heyd, G. E. Scuseria, and M. Ernzerhof, *J. Chem. Phys.* **118**, 8207 (2003).
- [25] N. Marzari and D. Vanderbilt, *Phys. Rev. B* **56**, 12847 (1997).
- [26] I. Souza, N. Marzari, and D. Vanderbilt, *Phys. Rev. B* **65**, 035109 (2001).
- [27] A. T. M. van Gogh, E. S. Kooij, and R. Griessen, *Phys. Rev. Lett.* **83**, 4614 (1999).
- [28] J. Hayoz, C. Koitzsch, M. Bovet, D. Naumovic, L. Schlapbach, and P. Aebi, *Phys. Rev. Lett.* **90**, 196804 (2003).
- [29] A. Pebler and W. E. Wallace, *J. Phys. Chem.* **66**, 148 (1962).
- [30] M. Mansmann and W. E. Wallace, *J. Phys. (Paris)* **25**, 454 (1964).
- [31] G. Renaudin, P. Fischer, and K. Yvon, *J. Alloys Compd.* **313**, L10 (2000).

- [32] G. S. Manyalia, R. Warmbier, and A. Quandt, *Comput. Mater. Sci.* **96**, 140 (2015).
- [33] G. L. Olcese, *J. Phys. F* **9**, 569 (1979).
- [34] H. G. Zimmer, H. Winzen, and K. Syassen, *Phys. Rev. B* **32**, 4066 (1985).
- [35] T. Doert, R. Asmuth, and P. Böttcher, *J. Alloys Compd.* **209**, 151 (1994).
- [36] Y. V. Voroshilov, M. I. Gurzan, Z. Z. Kish, and L. V. Lada, *Inorg. Mater.* **24**, 1265 (1988).
- [37] Generally for TSMs, the topological node is defined on a 2D manifold whose topological invariant is calculated in its codimensional space. For example, for a zero-dimensional DNP, the topological invariant is defined on the  $2 - 0 = 2$  dimension, i.e., on a sphere enclosing the DNP. In other words, the codimensionality of a DNP is 2. The codimensionality of an ideal DNS is  $2 - 2 = 0$ , so that its topological invariant is defined on a 0D point “enclosing” the 2D manifold as  $\Delta c$ .
- [38] S. Kobayashi, Y. Yamakawa, A. Yamakage, T. Inohara, Y. Okamoto, and Y. Tanaka, *Phys. Rev. B* **95**, 245208 (2017).
- [39] D. Y. Kim, R. H. Scheicher, and R. Ahuja, *Phys. Rev. Lett.* **103**, 077002 (2009).
- [40] F. Peng, Y. Sun, C. J. Pickard, R. J. Needs, Q. Wu, and Y. Ma, *Phys. Rev. Lett.* **119**, 107001 (2017).
- [41] J. N. Huiberts, R. Griessen, J. H. Rector, R. J. Wijngaarden, J. P. Dekker, D. G. de Groot, and N. J. Koeman, *Nature (London)* **380**, 231 (1996).
- [42] V. K. Fedotov, V. E. Antonov, I. O. Bashkin, T. Hansen, and I. Natkaniec, *J. Phys.: Condens. Matter* **18**, 1593 (2006).
- [43] <https://www.materialsproject.org/>.
- [44] P. A. Volkov and S. Moroz, [arXiv:1807.09170](https://arxiv.org/abs/1807.09170).